Temperature-sensitive colloidal phase behavior induced by critical Casimir forces

Minh Triet Dang,[1, a)] Ana Vila Verde,[2, b)] Van Duc Nguyen,[1, c)] Peter G. Bolhuis,[3, d)] and Peter Schall[1, e)]

[1)] *Van der Waals-Zeeman Institute, University of Amsterdam, Amsterdam, The Netherlands*

[2)] *Max Planck Institute of Colloids and Interfaces, Theory and Bio-Systems Department, Wissenschaftspark Golm, 14424 Potsdam, Germany*[f)]

[3)] *Van't Hoff Institute for Molecular Science, University of Amsterdam, Amsterdam, The Netherlands*

(Dated: 19 August 2013)

We report Monte Carlo simulations of phase behavior of colloidal suspensions with near-critical binary solvents using effective pair potentials from experiments. At off-critical solvent composition, the calculated phase diagram agrees well with measurements of the experimental system, indicating that many-body effects are limited. Close to the critical composition, however, agreement between experiment and simulation becomes poorer, signaling the increased importance of many-body effects. Both at and off the critical solvent concentration, the colloidal phase diagram is qualitatively similar to those of molecular systems and obeys the principle of corresponding states with one striking difference: it occurs in a narrow temperature interval of < 1°C below the solvent phase separation temperature.

[a)] Electronic mail: m.t.dang@uva.nl
[b)] Electronic mail: ana.vilaverde@mpikg.mpg.de
[c)] Electronic mail: ducnguyen@uva.nl
[d)] Electronic mail: p.g.bolhuis@uva.nl
[e)] Electronic mail: ps@peterschall.de
[f)] Also at the University of Minho, Physics Center, Campus de Gualtar, 4710-057 Braga, Portugal

I. INTRODUCTION

Colloidal suspensions have great potential for the assembly of nano and micron-scale structures, offering the opportunity for creating new functional materials (e.g. photonic crystals) by controlled aggregation. Successful assembly of such structures requires a high degree of control over the colloidal phase behavior and the kinetics of the growth process. Temperature, a crucial parameter in the control of atomic and molecular phase transitions, however, is usually a poor control parameter for colloidal interactions because most colloidal interaction potentials are fixed (set e.g. by the charge, the solvent refractive index, the concentration of salt or polymer used to induce depletion interaction between the particles). While specific systems such as microgels[1], DNA[2] and polymer-coated colloids[3] allow temperature control over colloidal interactions, a more generic route to temperature control of colloidal phase behavior is to suspend colloids in a near-critical binary liquid[4,5]. Close to the critical point of the binary solvent, concentration fluctuations become long-range, and their confinement between the surfaces of the particles leads to Casimir-type interactions known as critical Casimir forces[5–7]. Because the solvent fluctuations depend strongly on temperature, temperature provides a unique control parameter to tune these interactions. The advantage of this effect is its universality: as other critical phenomena, the scaling functions depend only on the internal symmetries, and are rather insensitive to the specific materials used[8,9]. This allows similar temperature control of phase behavior for many different colloids[10]. The question is then how to predict the phase behavior: because of the complexity of the critical Casimir interactions, the possible importance of many-body effects and the potential coupling between ions and solvent concentration fluctuations[11,12], there has been much discussion recently about the nature of the interactions and the relevant terms to be included[13–16]. Effective pair interactions have been discussed to provide a good description of colloidal phase behavior in reasonably dilute suspensions[13], and such effective interactions have been computed recently based on scaling functions calculated using the Ising model and combined with the Derjaguin approximation[13], and using simple solvent models with short-range interactions[17]. However, how close such effective potentials and the simulated phase behavior are to the experimental situation remains unclear. Therefore, the computation of a reliable phase diagram and the prediction of the real experimental phase behavior for the design of colloidal phases, remains desirable.

In this article, we use Monte Carlo (MC) simulations together with experimentally measured colloidal pair potentials to investigate the phase behavior of colloids in binary liquid solvents. This combination allows us to closely connect experimental observations and theoretical expectations of colloidal phase behavior in binary solvents. By using solvents with compositions both at and off the critical composition, we compare phase equilibria as a function of distance to the critical composition. We locate colloidal gas, liquid and solid phases as a function of temperature and colloid volume fraction. In contrast to standard MC simulations where the temperature T only enters via the thermal energy, $\beta^{-1} = k_B T$, with k_B Boltzmann's constant, our simulations account explicitly for the temperature-dependent potential. We find that at off-critical composition, the resulting colloidal phase diagram agrees quantitatively with experimental observations indicating that many-body interactions play a secondary role and that pair potentials are sufficient to describe the experimental system. In contrast, at the solvent critical concentration the calculated phase diagram shows larger deviation from the experimental one suggesting that many-body effects become more important. In both cases the calculated phase diagram has the characteristic topology associated with molecular potentials like the Lennard-Jones but occurs over a very narrow temperature range due to the strong temperature dependence of the solvent-mediated interactions. We finally show that the two systems exhibit similar gas-liquid coexistence curves when rescaled by the critical temperature and density, suggesting that, similarly to molecular gases, the principle of corresponding states is obeyed in systems with Critical Casimir forces.

II. METHODS

Simulating the phase behavior of the critical Casimir colloidal system requires a computationally efficient model. While in principle it is possible to compute the phase behavior from the ternary system of colloids in the liquid mixture, in practice this is prohibited by the large differences in length scales between the solvent molecules and the colloidal particles[13]. We therefore model the colloidal system as particles interacting with *effective* potentials which implicitly account for solvent effects. We thereby assume that many-body effects are negligible and that interactions are well-described by pair potentials. Our results below show that this choice yields very good agreement between the simulated phase diagram and our experimental observations for a binary solvent with off-critical composition, but suggest

that inclusion of many-body effects is desirable for solvent compositions close to the critical one.

We determine effective pair potentials from experimental measurement of the temperature-dependent pair distribution function $g(r;T)$ in dilute solutions; this distribution indicates the probability of finding two particles at a distance r relative to the ideal gas distribution. For dilute suspensions, the effective interaction potential follows directly from the relation $\beta U(r;T) \approx -\ln g(r;T)$. Because β always appears in combination with the potential $U(r;T)$ in the Boltzmann factor as $\beta U(r;T)$, it is this combination that is used in the simulations, rather than the potential U itself.

A. Colloidal system and potential measurement

We investigate two well-characterized systems[10,18] of poly-n-isopropyl acrylamide (PNIPAM) particles with a diameter of $\sigma = 500$ nm suspended in a near-critical quasi binary solvent composed of 3-methyl pyridine (3MP), water and heavy water[19,20]. The two systems differ only in the relative mass fractions w_x of the solvent components x (x=3MP, H_2O, D_2O), as shown in Table I. Solvent 1 is prepared at the critical composition of the 3MP - heavy water system, with a 3MP mass fraction of $w_{c,1} = 0.28$; solvent 2 is close to, but slightly off the critical composition of the 3MP - water - heavy water system[21], with a 3MP mass fraction of $w_{c,2} = 0.31$. The composition of solvent 2 is still sufficiently close to the critical one that critical density fluctuations occur[6,10,18].

TABLE I. Solvent mass fraction (w) and phase separation temperature (T_{cx}) of the two quasi-binary solvents used in the experiments. Solvent 1 is at its critical composition $w_{c,1} = 0.28$; solvent 2 is close to, but slightly off the critical composition $w_{c,2} = 0.31$.

	Solvent 1	Solvent 2
w_{3MP}	0.28	0.25
$w_{D_2O}/(w_{H_2O} + w_{D_2O})$	1	0.5
T_{cx} (°C)	39.5	52.2

The chosen experimental systems have the advantage that the particle refractive index

matches that of the solvent, allowing direct imaging of particles and determination of $g(r)$ deep in the bulk of the suspension. The particles are dyed, allowing us to image them under fluorescent illumination. The index match also minimizes van der Waals forces so that the only relevant particle interactions are the repulsive screened electrostatic, and the attractive critical Casimir interactions.[22] To measure the critical Casimir particle pair potential, a dilute suspension with a $\sim 2\%$ effective colloidal volume fraction was heated to temperatures just below T_{cx}, the solvent phase separation temperature. At each temperature, 3000 images of particle configurations were recorded to determine the average pair correlation function. The resulting experimental pair potentials are shown in Fig. 1. All temperatures are expressed in terms of $\Delta T = T - T_{cx}$, the temperature difference to the solvent phase separation. As expected, the attractive minimum of the potential deepens as the temperature approaches T_{cx}. This increasing minimum reflects the increasing critical Casimir force on approach to T_{cx}.

B. Potential model

To obtain closely spaced potentials that serve as input to the simulations, we use a simple potential model. We consider the effective colloid-colloid potential to consist of a screened electrostatic repulsion $U_{rep}(r)$ and a critical Casimir attraction $U_{attr}(r;T)$. This Ansats has been recently shown to provide a good description of the effective interparticle potential in systems similar to ours[5,11,23], although some discussion on this issue is ongoing[24]. For two particles of diameter σ at close center-center interparticle separation r, the repulsive electrostatic potential is[25]

$$U_{rep}(r) = A_{rep} \exp(-r/l_d) \tag{1}$$

where A_{rep} is the amplitude and l_d the Debye screening length. We note that in binary liquid mixtures, electrostatic interactions may have a more complex form than the simple exponential decay because of ion-solvent coupling arising from the different solubility of the ions in the two solvents[26–31]. Recent theoretical and experimental work has shown, however, that exponentially decaying electrostatic interactions are an excellent approximation for systems with symmetric boundary conditions[11] such as ours. The critical Casimir potential

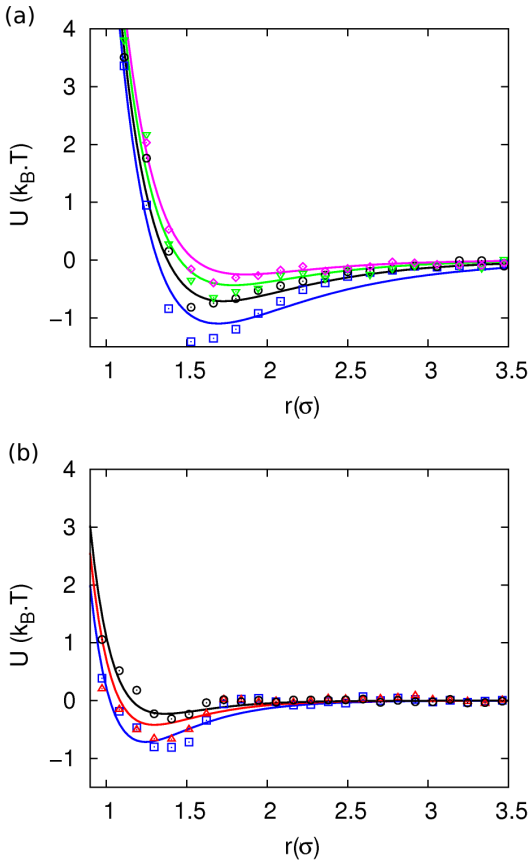

FIG. 1. Experimental (points) and fitted (lines) pair-potentials between colloids in system 1 (a) and system 2 (b), at $\Delta T = -0.3$°C (dark blue), $\Delta T = -0.35$°C (red), $\Delta T = -0.4$°C (black), $\Delta T = -0.5$°C (green) and $\Delta T = -0.6$°C (magenta). Distinct temperature sets were investigated for each system.

between two spherical particles can be approximated by

$$U_{attr}(r) = \frac{A_{attr}}{\xi} \exp(-r/\xi) \tag{2}$$

with ξ the correlation length of the solvent[5,6]. Prior theoretical work has shown that, for off-critical solvent compositions such as that of system 2, the universal scaling function for Casimir forces should also depend on a scaling variable that reflects the variation of the solvent correlation length with changes in the solvent composition[13,32]. As the solvent compositions investigated here are rather close to the critical composition, we neglect this additional dependence on solvent composition. We thus assume that near the critical point

of the binary solvent, the correlation length obeys the usual scaling relation

$$\xi = \xi_0 \left(1 - \frac{T}{T_{cx}}\right)^{-0.63} \tag{3}$$

where ξ_0 is the solvent correlation length far from the solvent phase separation temperature[33]. Thus, the Casimir potential range, set by the correlation length ξ, as well as the amplitude, $A_{attr}/\xi \sim k_B T$, depend on experimental temperature[5,6]. To obtain values of ξ_0, A_{rep} and l_d, we fit the analytical expression

$$U(r;T) = U_{rep}(r) + U_{attr}(r;T) \tag{4}$$

to the experimentally measured $U(r;T)$ as shown in Fig. 1. Using the best set of values, we are able to fit the entire set of potentials $U(r;T)$ with one single set of parameters reasonably well. However, deviations between the measurements and the fits are clearly visible; these occur due to possible effects of ion-concentration coupling and particle softness that are not accounted for in the model. The largest deviations occur at short interparticle distances; these deviations arise from the fact that the PNIPAM particles are soft and thus easily compressed below their diameter at infinite dilution (note that the potentials shown in Fig. 1 are still finite at $r < \sigma$), and the chosen potential form does not account for this effect. To estimate whether this deviation has a significant effect on the computed phase behavior, we calculate the normalized second virial coefficients B_2^* for both fitted and measured potentials for system 2. According to Noro and Frenkel's extended principle of corresponding states, the

TABLE II. B_2^* coefficients for the experimental and fitted potentials for system 2 at three different temperatures.

	ΔT (°C)		
	-0.40	-0.35	-0.30
experiment	0.3	-1.0	-2.5
fitted	-0.02	-1.2	-3.3

second virial coefficient is a rough estimator of the phase behavior that should arise from a given potential[34,35]: a B_2^* that is positive correlates with net repulsion between the particles, indicating that a phase transition should not occur; a B_2^* that is close to zero indicates

little net attraction or repulsion between the particles, so a phase transition is not expected. Phase transitions are expected to occur when B_2^* becomes smaller than -1.5. It follows that if the experimental and fitted potentials at the same temperature lead to second virial coefficients of the same sign and comparable magnitude, the phase diagrams resulting from those potentials are expected to have the same topology and show only small quantitative differences. We compare the normalized second virial coefficients for system 2 in Table II: At the lowest temperature ($\Delta T = -0.40$°C), the calculated B_2^* coefficients for the fitted and experimental potentials are close to zero, indicating that phase transitions should not yet occur. This is in agreement with both experiment and simulation: at this temperature, phase transitions do not occur in either case. At the two highest temperatures for which the potentials were measured experimentally ($\Delta T = -0.35; -0.30$°C) the B_2^* coefficients for both fitted and experimental potentials are negative and of comparable magnitude, so we expect that the fitted potentials will lead to the qualitatively correct phase behavior and that phase separation will occur when $\Delta T < -0.3$°C. These findings suggest that approximating the experimental potentials with the fitted ones will result in a calculated phase diagram with the correct topology. The results shown below demonstrate that this is indeed the case. We list the values of the fitting parameters in Table III. The potentials for system 1 are significantly longer-range than for system 2, a consequence of the solvent composition of system 1 being nearer to the critical one.

TABLE III. Model parameters.

Parameter	System 1	System 2
A_{rep} (k_BT)	0.1046×10^4	0.1994×10^4
l_d (σ)	0.2206	0.153
A_{attr} $(k_BT\sigma)$	0.1188×10^2	0.170×10^2
ξ_0 (σ)	0.908999×10^{-2}	0.418×10^{-2}

C. Simulation details

To obtain a complete phase diagram, we use the analytic expression of the potential (eqs. 1, 2 and 3) together with the fit parameters shown in Table III to produce a set of

closely-spaced potentials in a wide temperature range. We investigate gas-liquid coexistence using Gibbs Ensemble MC[36,37] and liquid-crystal coexistence using Kofke's Gibbs-Duhem integration technique[38]. For the simulations, we cut off the potentials at 4.5σ (system 1) and 3.5σ (system 2); we found that due to the rather long range of the potentials, this unusually large cut-off radius was required to obtain meaningful results. Further details of the simulations are given in the Supplementary Information.

III. RESULTS AND DISCUSSION

A. Phase diagram

The computed phase diagrams are shown in Fig. 2. For both systems, the critical Casimir potential induces a separation into a dilute gas and a dense liquid phase at temperatures close to T_{cx}. As the temperature decreases, the critical Casimir potential becomes weaker, and the gas-liquid coexistence region shrinks, until the binodal curves end in a critical point. At even lower temperatures, the particles stay homogeneously suspended. Very similar behavior is observed in the experiments[10,18] for system 2: at $\Delta T = -0.35$°C the colloidal particles remained uniformly suspended, while at $\Delta T = -0.30$ and -0.25°C, phase separation in gas and liquid was observed. As an example, we show confocal microscope images of the observed gas-liquid and gas-crystal phase coexistence in Fig. 2c and d. The three-dimensional imaging by confocal microscopy allowed us to measure the gas and liquid volume fractions directly by particle counting; these volume fractions together with their error margins are indicated in the simulated phase diagram. The data shows reasonable agreement with the phase diagram of system 2 given the large uncertainty in the determination of ϕ and ΔT. This agreement suggests that many-body effects are limited, even at high colloid volume fractions.

For system 1, the agreement between experiment and simulation is less good, as reflected e.g. in the shift of the calculated gas-liquid curve towards lower values of ΔT compared to the experimental points. This shift indicates that the fitted potentials overestimate the colloidal interactions, likely because the fitted potentials do not include many-body terms which often decrease the net attractive force between particles[39]. We conclude that the longer range of the interaction at similar interaction magnitude makes many-body effects more pronounced at the critical solvent composition, in agreement with recent mean field

estimates of many-body Critical Casimir forces in a system of two colloids near a wall[40]. We note, however, that for the few colloid-colloid-wall configurations investigated in that study, many-body forces often increased rather than decreased the colloid-colloid attraction. The downward shift of the calculated gas-liquid curve relative to the experimental data observed here suggests that many-body forces in systems of many colloids decrease the net attractive force between the colloids. Our results thus highlight the need for a more detailed study of many-body contributions in critical Casimir interactions.

We further investigate the occurrence of crystal-liquid equilibria. As the Gibbs ensemble is not easily applied to solid-liquid coexistence, we instead employ Kofke's Gibbs-Duhem integration technique[38]. Here, the full coexistence curve is computed by numerically integrating the Gibbs-Duhem equation (or equivalently, the Clausius-Clapeyron equation) starting from a known reference coexistence point as described elsewhere[41]. The resulting fluid-solid coexistence curve, shown in Fig. 2, connects well with the gas-liquid phase boundary: the two curves intersect at $\Delta T = -0.312°\mathrm{C}$ (system 1) and $\Delta T = -0.248°\mathrm{C}$ (system 2), the triple points, where the liquid-crystal coexistence pressure almost vanishes[42]. These observations are again consistent with our experiments: at temperatures ΔT between -0.25 and $-0.20°\mathrm{C}$, face-centered cubic (fcc) crystals formed inside the liquid drops; at $\Delta T = -0.20°\mathrm{C}$, the aggregates consisted entirely of fcc crystals (Fig. 2c), with a volume fraction of $\phi \sim 0.5$, in agreement with the simulations (see Fig. 2). Our results indicate that the attractive range of the potential significantly affects the crystal-liquid coexistence, with longer range potentials bending the curves towards lower density and narrowing the coexistence region.

Finally, we use Gibbs-Duhem integration to investigate the region of gas-crystal coexistence. Starting from the crystal configurations obtained for the crystal-liquid equilibria, we continue the integration up to $\Delta T = -0.1°\mathrm{C}$ while imposing the additional condition that the coexistence-pressure is zero. Similarly to what we observe for crystal-liquid equilibria, we find that longer range potentials shift gas-crystal coexistence towards lower density.

The phase diagrams shown in Fig. 2 mirror the well-known gas-liquid-solid phase diagram of Lennard-Jones systems[43,44], lattice-based Ising models[45], and systems with square-well potentials[46,47]. The diagrams are inverted with respect to the known phase diagram of Lennard-Jones systems, because βU becomes stronger as we approach the solvent phase separation from below, instead of βU becoming weaker with increasing temperature, as is the case in Lennard-Jones systems. The small temperature range over which the gas-liquid

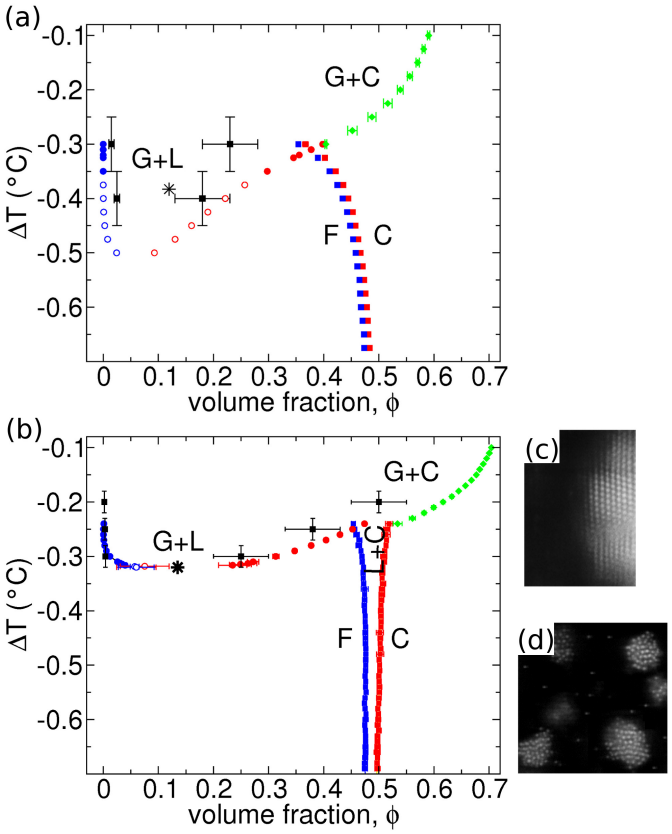

FIG. 2. Colloidal phase diagram induced by the critical Casimir forces for system 1 (a) and system 2 (b), and snapshots of confocal microscope observations of system 2 at $\Delta T = -0.2$°C (c) and $\Delta T = -0.3$°C (d). The circles denote the gas-liquid coexistence curve; the empty circles indicate the sections of the gas-liquid coexistence curve where finite size effects are larger. The star indicates the gas-liquid critical point calculated as described in the main text. For the estimated critical temperatures, the normalized second virial coefficients are $B_2^* = -14.2$ and $B_2^* = -2.3$ for system 1 and 2, respectively. The blue and red squares denote the fluid-crystal (F-C) and the green diamonds the gas-crystal (G+C) coexistence curves. The black squares and error bars are coexistence points of gas-liquid (system 1: $\Delta T = -0.3, -0.4$°C; system 2: $\Delta T = -0.3, -0.25$°C) and gas-crystal (system 2: $\Delta T = -0.20$°C) from experiment.

curves extend reflects the explicit strong temperature dependence of the potential. This temperature range is larger for system 1 (0.2 °C) than for system 2 (0.1 °C) because, since the potentials are longer-range in system 1, the net interaction of each particle with the rest of the system is significant while the potential magnitude is still small. Further consequences of the longer potential range are the shift of the apparent critical point and the liquid-crystal

coexistence to lower volume fractions, i.e. larger interparticle separations.

B. Scaling at the colloidal gas-liquid critical point

It is interesting to characterize the critical scaling near the gas-liquid critical point. For short-range potentials and a scalar order parameter such as the density considered here, three-dimensional Ising scaling is expected in the absence of finite size effects; however, mean field scaling is observed otherwise[33,46]. The scaling behavior thus gives us another indication of the potential range and finite size effects. To investigate it, we calculate the difference between gas and liquid volume fractions, $M(T) = \phi_l - \phi_g$, to test a scaling relation of the form

$$M(T) = B(T - T_C)^{\beta_c} \tag{5}$$

where β_c is the critical exponent and B is an unknown fitting parameter[48]. We plot the normalized order parameter, $M^{1/\beta_c}/M_{max}^{1/\beta_c}$, as a function of ΔT in Fig. 3 using the two relevant values of β_c[45,49]: the classical or mean field $\beta_c = 1/2$, and the non-classical $\beta_c = 0.325$ for the 3D Ising model. The curves are normalized by their maximum value, M_{max}^{1/β_c}, to bring them in the same numerical range for more convenient display. We find that system 2 shows indeed the expected 3D Ising scaling, as indicated by the consistent linear relation of the gray squares shown on the right hand side. In contrast, for system 1, a crossover from 3D Ising scaling to mean-field scaling is observed: the linear dependence for $\beta_c = 0.325$ crosses over to a linear dependence for $\beta_c = 0.5$ at temperatures $\Delta T \sim 0.35°C$, indicating that far from the critical temperature the system follows the expected 3D Ising scaling, but as the temperature approaches the critical one, a crossover to mean-field scaling occurs. Similar crossover behavior has been observed for 2D square-well[46] or Lennard-Jones[44] systems; it indicates that, despite the large box size used in the simulations, the correlation lengths are already comparable to the simulation box size. The crossover behavior signals that the calculated gas-liquid curve for $\Delta < -0.4$°C, indicated by the empty symbols in Fig. 2 (a), reflects marked finite size effects. This again highlights the longer-range nature of the interactions in system 1 at the solvent critical point.

The observed Ising scaling can be used to estimate the gas-liquid critical point. To determine the critical temperature, we extrapolate the linear fits for $\beta_c = 0.325$ to $M(T) = 0$. Furthermore, to determine the critical volume fraction, ϕ_C, we fit ϕ_l and ϕ_g to the law of

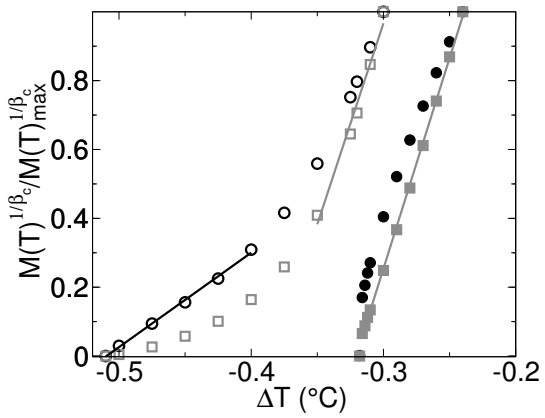

FIG. 3. Volume fraction differences scaled with $1/\beta_c$ against experimental temperatures, for different critical exponents: $\beta_c = 1/2$ (black points), and $\beta_c = 0.325$ (grey points). Empty symbols correspond to system 1, filled ones to system 2. The lines are linear fits to the points in the same x- and y-range as the lines.

rectilinear diameters[50]

$$\frac{\phi_l + \phi_g}{2} = \phi_C + A(T - T_C) \tag{6}$$

using T_C as input and A as a fitting parameter. We obtain $\Delta T_{C,1} = -0.38°\text{C}$ and $\phi_{C,1} = 0.12$ for system 1, and $\Delta T_{C,2} = -0.32°\text{C}$ and $\phi_{C,2} = 0.13$ for system 2. The resultant critical point, indicated by the star in each phase diagram in Fig. 2, agrees well with the calculated gas-liquid curve for system 2. The calculated critical temperature also agrees well with that estimated from Noro and Frenkel's principle of corresponding states[35], as discussed above. However, larger deviations between the estimated critical point and the calculated gas-liquid curve occur for system 1 as a consequence of the finite size effects associated with the longer range of the potential. The stronger finite size effects present in system 1 imply that the uncertainty associated with the critical point estimated from Eqs. 5 and 6 is larger for this system than for system 2. This larger uncertainty explains why the normalized second virial coefficient at the critical temperature for system 1, $B_2^* = -14.2$, is much further from the expected value[35], $B_2^* = -1.5$ than that for system 2 ($B_2^* = -2.3$).

The universality of the scaling behavior is reflected in the principle of corresponding states: all molecular gases obey the same behavior if their thermodynamic variables are scaled by the critical values. To highlight the principle of corresponding states for our systems, in Fig. 4 we plot the reduced temperature as a function of reduced density and

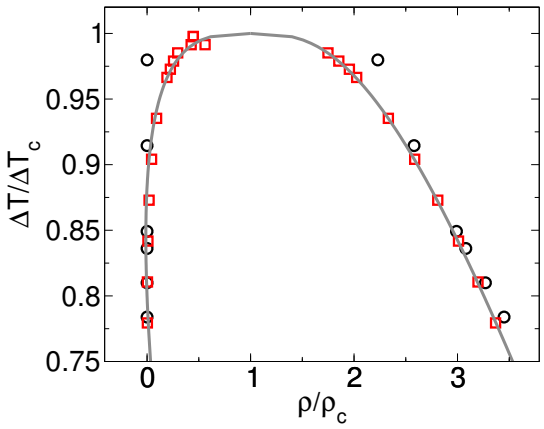

FIG. 4. Scaled gas-liquid coexistence curves for system 1 (black) and system 2 (red). Only the points following 3D-Ising scaling are shown. The grey curve is the fit resulting from the scaling relation and the law of rectilinear diameters using parameters for system 2.

compare the two colloidal systems. Far from the critical point, where finite size effects are minimum, the scaled gas-liquid coexistence curves for both systems coincide, indicating that the principle of corresponding states applies also to Critical Casimir systems, in qualitative agreement with recent experiments[18]. To highlight this correspondence, we have added a fit obtained[41] by combining the scaling relation and the law of rectilinear diameters as discussed above with the constants $A = 1.3125$, $B = 1.067$ and $\beta_c = 0.325$.

IV. CONCLUDING REMARKS

By computing the phase behavior of colloids in critical binary solvents, we have demonstrated the colloidal assembly control arising from critical Casimir forces with temperature as the control parameter. The phase diagram that we obtain is similar to that of molecular systems, but occurs over a small temperature interval $\Delta T < 1°C$ below the solvent phase separation temperature. We identified an interesting dependence on the solvent composition: further from the critical concentration of the binary solvent, the good agreement between the simulation phase diagram and experimental data suggests that the critical Casimir interactions between colloids are sufficiently well-described by two-body potentials. As the critical concentration of the binary solvent is approached, however, many-body effects become significant and should be included for better agreement between experiment and simulation. Significant improvement may be obtained already with the inclusion of a three-body term.

In principle, this term could be obtained from experiment, e.g., by calculating the 3-particle correlation function from confocal images of the system. The technical difficulties involved in obtaining the necessary large numbers of high quality confocal images precluded us from doing so here. The crossover from 3D Ising to mean field scaling despite the large simulation boxes indicates that correlation lengths are large. Practically, this observation implies that accurate determination of critical properties will require unusually large simulation boxes. In contrast to other temperature-dependent colloid-colloid potentials, the critical Casimir effect allows temperature control of colloidal phases in a new, reversible and universal fashion. The temperature range within which the colloidal phase transitions occur can be tuned by changing the composition of the binary solvent, but will typically be no larger than a few degrees. The narrowness of the relevant temperature range implies that colloidal interactions with lower sensitivity to temperature, such as those occurring, e.g., in polymer coated colloids, remain approximately constant, which facilitates control over the experimental systems. The combined experimental and simulation study presented here lays the ground to a more quantitative comparison of the phase behavior of colloids in binary solvents. Future directions of this fascinating system include the use of patterned particles to obtain anisotropic critical Casimir interactions for more complex structures and phase behavior. Furthermore, the reversible temperature control opens opportunities to use temperature gradient and zone melting techniques to grow perfect equilibrium structures, as e.g. required for photonics, in analogy to the growth of high-quality atomic crystals.

ACKNOWLEDGMENTS

This work was supported by the Foundation for Fundamental Research on Matter (FOM). P.S. acknowledges support from the Innovational Research Incentives Scheme (VIDI grant) of the Netherlands Organization for Scientific Research (NWO). A.V.V. acknowledges financial support by the department of Theory and Bio-Systems at the Max Planck Institute of Colloids and Interfaces. We thank A. Maciolek and D.T.F. Mohry for helpful discussions.

REFERENCES

[1]R. Pelton, Adv. Colloid Interface Sci. **85**, 1 (2000).

[2]M. E. Leunissen, R. Dreyfus, F. C. Cheong, D. G. Grier, R. Sha, N. C. Seeman, and P. M. Chaikin, Nat. Mater. **8**, 590 (2009).

[3]J. Wu, B. Zhou, and Z. Hu, Phys. Rev. Lett. **90**, 048304 (2003).

[4]H. Guo, T. Narayanan, M. Sztuchi, P. Schall, and G. Wegdam, Phys. Rev. Lett. **100**, 188303 (2008).

[5]D. Bonn, J. Otwinowski, S. Sacanna, H. Guo, G. Wegdam, and P. Schall, Phys. Rev. Lett. **103**, 156101 (2009).

[6]C. Hertlein, L. Helden, A. Gambassi, S. Dietrich, and C. Bechinger, Nature **451**, 172 (2008).

[7]A. Gambassi, A. Maciolek, C. Hertlein, U. Nellen, L. Helden, C. Bechinger, and S. Dietrich, Phys. Rev. E **80**, 061143 (2009).

[8]D. Beysens and D. Estève, Phys. Rev. Lett. **54**, 2123 (1985).

[9]M. E. Fisher and P. G. De Gennes, C. R. Acad. Sci. Paris B **287**, 207 (1978).

[10]P. B. Shelke, V. D. Nguyen, A. V. Limaye, and P. Schall, Adv. Mater. **25**, 1499 (2013).

[11]M. Bier, A. Gambassi, M. Oettel, and S. Dietrich, EPL (Europhysics Letters) **95**, 60001 (2011).

[12]U. Nellen, J. Dietrich, L. Helden, S. Chodankar, K. Nygard, J. Friso van der Veen, and C. Bechinger, Soft Matter **7**, 5360 (2011).

[13]S. D. T. F. Mohry, A. Maciolek, J. Chem. Phys. **136**, 224902 (2012).

[14]R. Okamoto and A. Onuki, Phys. Rev. E **84**, 051401 (2011).

[15]R. Okamoto and A. Onuki, J. Chem. Phys. **136**, 114704 (2012).

[16]S. Samin and Y. Tsori, J. Chem. Phys. **136**, 154908 (2012).

[17]N. Gnan, E. Zaccarelli, P. Tartaglia, and F. Sciortino, Soft Matter **8**, 1991 (2012).

[18]V. D. Nguyen, S. Faber, Z. Hu, G. H. Wegdam, and P. Schall, Nat. Commun. **4**, 1584 (2013).

[19]T. Narayanan, A. Kumar, and E. S. R. Gopal, Phys. Lett. A **155**, 276 (1991).

[20]D. Beysens and T. Narayanan, J. Stat. Phys. **95**, 997 (1999).

[21]J. Cox, J. Chem. Soc. , 4606 (1952).

[22]We note that as the Hamaker constant vanishes only for one specific frequency, Van der Waals forces strictly vanish only for this particular frequency. However, experimental measurements show that at the rather large interparticle distances occurring here, Van der Waals interactions are not relevant.

[23]D. Bonn, G. Wegdam, and P. Schall, Phys. Rev. Lett. **105**, 059602 (2010).

[24]A. Gambassi and S. Dietrich, Phys. Rev. Lett. **105**, 059601 (2010).

[25]J. Israelachvilli, *Intermolecular and Surface Forces* (Wiley, New York, 1976).

[26]V. Nabutovskii, N. Nemov, and Y. G. Peisakhovich, Molecular Physics **54**, 979 (1985).

[27]A. Onuki and H. Kitamura, J. Chem. Phys. **121**, 3143 (2004).

[28]A. Onuki, Phys. Rev. E **73**, 021506 (2006).

[29]A. Ciach and A. Maciolek, Phys. Rev. E **81**, 041127 (2010).

[30]F. Pousaneh and A. Ciach, J. Phys: Condens. Matter , 412101 (2011).

[31]F. Pousaneh, A. Ciach, and A. Maciolek, Soft Matter **8**, 7567 (2012).

[32]T. F. Mohry, A. Maciolek, and S. Dietrich, J. Chem. Phys. **136**, 224903 (2012).

[33]R. K. Pathria, *Statistical Mechanics*, 2nd ed. (Butterworth-Heinemann, 2001).

[34]G. A. Vliegenthart and H. N. W. Lekkerkerker, J. Chem. Phys. **112**, 5364 (2000).

[35]M. G. Noro and D. Frenkel, J. Chem. Phys. **113**, 2941 (2000).

[36]D. Frenkel and B. Smit, *Understanding Molecular Simulation, Second Edition: From Algorithms to Applications* (Academic Press, San Diego, California, USA, 2001).

[37]A. Z. Panagiotopoulos, Mol. Phys. **61**, 813 (1987).

[38]D. A. Kofke, J. Chem. Phys. **98**, 4149 (1993).

[39]J. N. Israelachvili, *Intermolecular and surface forces*, second edition ed. (Academic press, 1991).

[40]T. G. Mattos, L. Harnau, and S. Dietrich, J. Chem. Phys. **138**, 074704 (2013).

[41]See Electronic Supplementary Information for details of the calculation of the second virial coefficient, computational details of the Gibb-Duhem and Gibbs ensemble simulations, and the expressions used to fit the gas-liquid coexistence curve.

[42]J. Q. Broughton and X. P. Li, Phys. Rev. B **35**, 9120 (1987).

[43]B. Smit, P. Desmedt, and D. Frenkel, Mol. Phys. **68**, 931 (1989).

[44]A. Z. Panagiotopoulos, Int. J. Thermophys. **15**, 1057 (1994).

[45]K. K. Mon and K. Binder, J. Chem. Phys. **96**, 6989 (1992).

[46]J. R. Recht and A. Z. Panagiotopoulos, Mol. Phys. **80**, 843 (1993).

[47]L. Vega, E. de Miguel, L. F. Rull, G. Jackson, and I. A. McLure, J. Chem. Phys. **96**, 2296 (1992).

[48]J. S. Rowlinson and B. Widom, *Molecular Theory of Capillarity* (Clarendon Press, Oxford, 1982).

[49]K. Binder and E. Luijten, Phys. Rep. **344**, 179 (2001).

[50]J. S. Rowlinson and F. L. Swinton, *Liquids and Liquid Mixtures*, 3rd ed. (Butterworth, London, 1982).